Defective Nanographenes Containing Seven-Five-Seven (7–5–7)-Membered Rings

Fei, Y.; Fu, Y.; Bai, X.; Du, L.; Li, Z.; Komber, H.; Low, K.-H.; Zhou, S.; Lee Phillips, D.; Feng, X.; Liu, J.;

Originally published:

January 2021

Journal of the American Chemical Society 143(2021), 2353-2360

DOI: https://doi.org/10.1021/jacs.0c12116

Defective Nanographenes Containing Seven-Five-Seven (7-5-7) Membered Rings: Anti-aromaticity or Pro-aromaticity?

Yiyang Fei, Yubin Fu, Zichao Li, Hartmut Komber, Shengqiang Zhou, Xinliang Feng, Junzhi Liu*

Abstract: Defects have been observed in graphene and are expected to play a key role in tailoring its optical, electronic, and magnetic properties. However, most of the studies focused on the structural characterizations, the implications of topological defects on the physicochemical properties of graphene remains poorly understood. Here, we demonstrate the bottom-up synthesis of two novel nanographenes (**1** and **2**) with well-defined defect, in which seven-five-seven (7-5-7) membered rings are introduced into their sp^2 carbon frameworks. From the X-ray crystallographic analysis, compound **1** adopts a nearly planar structure; compound **2**, with an additional five-membered ring compared with **1**, possesses a slightly saddle-shaped geometry. Detailed experimental and theoretical investigations elucidate that both defective nanographenes **1** and **2** exhibit anti-aromatic feature at the ground state and display high stability under ambient conditions, which contrasts with the reported unstable biradicaloid nanographenes containing heptagons.

Graphene is an atomically thick sheet composed of a hexagonal network of sp^2-hybridized carbon atoms with exceptional electronic and optical properties, as well as a credible starting point of materials for new disruptive technologies across a wide range of fields.[1-4] However, graphene is a semimetal without bandgap and cannot be directly used for electronics. This makes it crucial to find a way of opening the bandgap for graphene-based nanoelectronics.[5] The most prominent way is to locally confine the electrons what renders stripes of graphene, so called graphene nanoribbons (GNRs) as a semiconducting materials.[6-9] Another pathway to influence the electronic structure of graphene is introducing the imperfections/defects in the basal plane of graphene.[10] Theoretical calculations have described that topological defects in graphene significantly affect its optical, electronic, and magnetic properties.[11] The typical stable graphene defects, including atom dislocation (pentagon-heptagon pair, azulene unit, Fig. 1a), Stone-Wales (SW) defects (point defects, Fig. 1b), vacancies (single and multiple), and one-dimensional defects (line defects), have been predicted and also experimentally observed.[10] From the viewpoint of energetic stability, the pentagon-heptagon pair (5-7 rings) is one of the reasonable defect models which can be generated in a graphene layer due to the atom dislocation (Fig. 1a).[12,13] Generally, the topological defects can be introduced into graphene or related 2D materials by electron irradiation, or they are formed during the high temperature growth.[14,15] Despite the growing number of experimental observations, the defects in graphene are still not well understood, especially for evaluating and studying the effect of topological defects on the optical, electronic and magnetic properties.[16] Therefore, the investigation of the chemical and physical properties depending on the defined defect plays an important role in defect engineering of graphene, which can provide insight into understanding the structure-property relationship of graphene.

Recently, embedding of pentagon-heptagon pair (an azulene unit) into large π-conjugated polycyclic hydrocarbon aromatics (PAHs) or nanographenes have been developed. For instance, we reported the synthesis of open shell nanographenes containing a pair of azulene units both in the solution and on the surface (Fig. 1c).[17] Contorted PAHs containing two azulene cores were synthesized by Mastalerz *et al.* through cyclopent- and cyclohept-annulations.[18] A non-benzenoid PAH containing two pentagons and two heptagons with high hole-mobility was reported by Zhang and co-authors.[19] Konishi and Yasuda *et al.* reported an open-shell non-alternant isomer of bisanthene with heptalene structure (Fig. 1c).[20] Chi's group demonstrated the synthesis of an azulene-embedded nanographene due to the unexpected naphthalene to azulene rearrangement during the Scholl reaction.[21] Very recently, a cove-edged helical nanographene containing contiguous azulene units was synthesized by Takasu and co-workers.[22] Despite these achieved progress, the synthesis of non-alternant topology in graphene nanostructures,[23-26] such as the seven-five-seven (7-5-7) membered rings (Fig. 1d), still remain elusive due to the lack of a facile synthetic approach[27] and the unexpected rearrangement.[21,28,29]

[a] Y. Fei, Dr. J. Liu
Department of Chemistry and State Key Laboratory of Synthetic Chemistry, The University of Hong Kong, Rokfulam Road, Hong Kong, P. R. China

E-mail: juliu@hku.hk

[b] Y. Fu, Prof. Dr. X. Feng
Centre for Advancing Electronics Dresden (cfaed), Faculty of Chemistry and Food Chemistry, Technische Universität Dresden, 01062 Dresden, Germany

[b] Z. Li, Dr. S. Zhou
Helmholtz-Zentrum Dresden-Rossendorf, Institute of Ion Beam Physics and Materials Research, Bautzner Landstrasse 400, 01328 Dresden, Germany

[d] Dr. H. Komber

Leibniz-Institut für Polymerforschung Dresden e. V. Hohe Straße 6, 01069 Dresden, Germany

Supporting information for this article is given via a link at the end of the document.

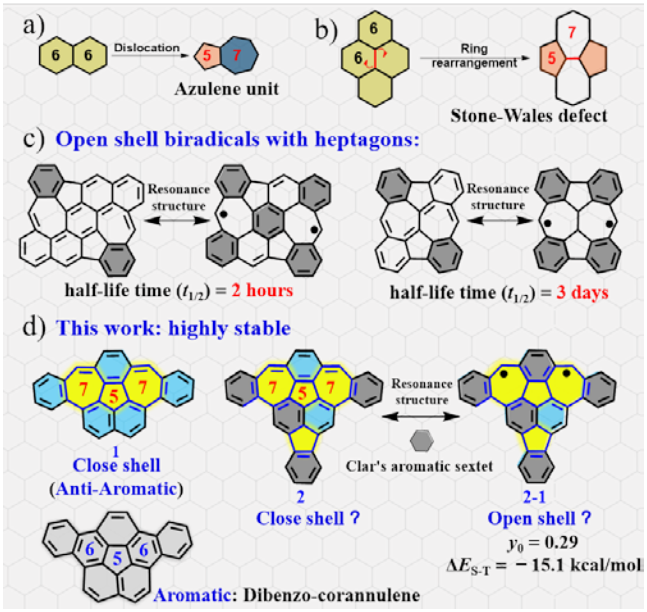

Figure 1. (a) Azulene unit. (b) Stone-Wales defect. (c) Recent examples of nanographenes with open-shell character containing heptagons. (d) The defective nanographenes with 7-5-7 membered rings reported in this work.

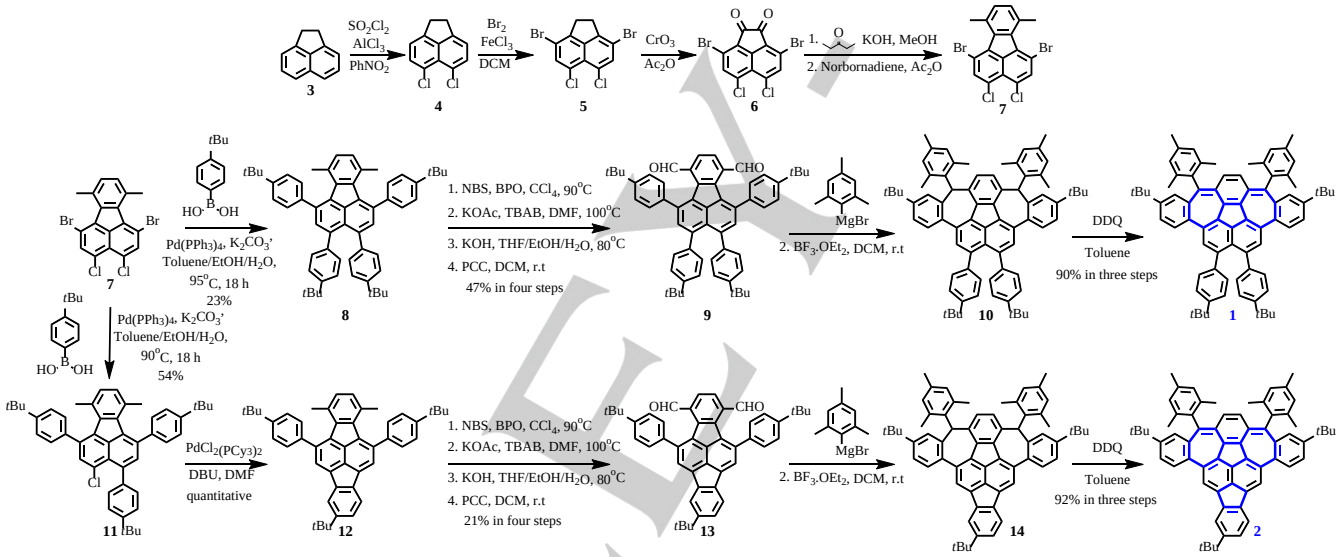

Scheme 1. Synthetic routes toward compounds **1** and **2** with 7-5-7 membered rings.

Herein, we demonstrate an efficient synthetic strategy towards two unprecedented defective nanographenes containing 7-5-7 membered rings (**1** and **2**, Fig. 1d), in which there is an additional five-membered ring in **2** compared with **1**. Single crystal X-ray analysis unequivocally reveals the embedded non-alternant topology in **1** and **2**. Compound **1** adopts a nearly planar structure while **2** possesses a slightly saddle-shaped geometry with a torsion angle of 20.6º and 21.4º, respectively (Fig. 3). Interestingly, ring A in **1** (Fig. 3a), which lying on the 7-5-7 membered rings, possesses pronounced bond alternation for the *p*-quinodimethane framework (Fig. 3c), indicating its antiaromaticity, in contrast to the aromatic dibenzo-corannulene with 6-5-6 membered rings (Fig. 1d). Ring A in **2** (Fig. 3b) does not feature the bond alternation of the *p*-quinodimethane unit as in **1**, suggesting its open shell biradical character (Fig. 1d).[30-32] Indeed, from the density functional theory (DFT) calculations, compound **1** displays close shell (anti-aromatic) feature (see below), while **2** has a moderate singlet biradical character (y_0 = 0.29, UHF method) with a large singlet-triplet energy gap (ΔE_{S-T} = −15.1 kcal/mol, UCAM-B3LYP/6-31G(d)). However, compound **2** manifested intensive nuclear magnetic resonance (NMR), silent electron paramagnetic resonance (EPR) signal, and absence of a low-lying excited singlet state dominated by the doubly excited configuration. All these experimental results indicate that compound **2** features the close shell anti-aromatic character at the ground state (Fig. 1d). The resultant anti-aromatic nanographenes **1** and **2** exhibit high stability over months, this feature stands in contrast with the reported unstable open shell nanographenes containing heptagons. For instance, the half-life time of difluoreno-[1,9,8-*alkj*:1`,9`,8`-*gfed*]heptalene is only 3 days (Fig. 1c).[20] Our work reported herein provides a new line to the synthesis of air-stable anti-aromatic nanographenes with non-alternant topology and enables control of their electronic structures.

The synthetic routes toward compounds **1** and **2** are described in Scheme 1. First, the key building block 1,6-dibromo-3,4-dichloro-7,10-dimethylfluoranthene (**7**) was synthesized from the starting compound 1,2-dihydroacenaphthylene (**3**) in 4 steps through chlorination, bromination, oxidation, and Diels-Alder reaction.[33] Then, compound **8** was obtained via the Suzuki coupling of **7** and (4-(*tert*-butyl)phenyl)boronic acid in 23% yield. The methyl groups in **8** were transformed into dialdehydes by bromination, esterification, hydrolysis, and Swern oxidation, to afford compound **9** in 47% yield. Dihydro-precursor **10** was synthesized by treatment of **9** with mesitylmagnesium bromide (MesMgBr) and then Friedel-Crafts cyclization. Dehydrogenation of **10** using 2,3-dichloro-5,6-dicyano-1,4-benzoquinone (DDQ) provided the purple target compound **1** with the yield of 90% in three steps. On the other hand, compound **11** was achieved through the selective Suzuki coupling of **7** and (4-(*tert*-butyl)phenyl)boronic acid in 54% yield. Subsequently, Pd-induced Heck reaction of **11** gave **12** (quantitative). Following the similar synthetic strategy, compound **2** was successfully synthesized as purple powder with the yield of 92% in three steps. The chemical structures of **1** and **2** were confirmed by high-resolution mass spectrometry (HR MS), NMR analysis (both see the Supporting Information) and X-ray single crystal analysis (vide infra).

Although compound **2** possesses open shell biradical character (y_0 = 0.29) from the theoretical simulation, the ^{1}H NMR spectrum of **2** showed well-resolved signals at room temperature (Fig. S12), in sharp contrast to the most reported biradicaloids,[34-37] which demonstrated broadened signals at room temperature. Moreover, compound **2** did not result in broadening peak even heating it in toluene-d_8 up to 90 °C (Fig. S13). This feature of **2** is likely due to its large singlet-triplet energy gap ($\Delta E_{S\text{-}T}$).[38,39] Obviously, **2** does not display a low-energy-lying thermally accessible triplet state in this range of temperatures.[38,39] The solid powder of both compounds **1** and **2** donot display any EPR signal at the room temperature. In addition, superconducting quantum interfering device (SQUID) measurement was carried out with the powder sample of **2** up to 400 K (Fig. 2). However, the SQUID result did not show an increasing susceptibility even above 400 K,[38] which further suggests its large $\Delta E_{S\text{-}T}$. From the theoretical calculation (UCAM-B3LYP/6-31G(d)), the value of $\Delta E_{S\text{-}T}$ is estimated to be −15.1 kcal/mol for **2**, higher than that of the reported biradicaloids.[34-37] Moreover, from the calculated result by Bleaney–Bowers equation with high spin energy gap ($\Delta E_{S\text{-}T}$ = −15.1 kcal/mol) (Fig. 2), it is known that the increase in magnetic molar susceptibility above ~750 K and the result below 400 K is in well agreement with fitting curves. These NMR, EPR and SQUID measurements suggest that it is more reasonable to describe **2** as close shell anti-aromatic compound at the ground state.

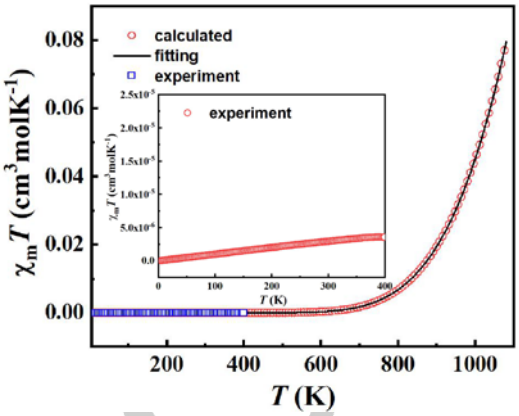

Figure 2. Thermal variation of the χ_mT of compound **2** in the temperature range 5–400 K from SQUID measurements and calculated χ_mT in the temperature range 5–1080 K. Insert: enlarge the experimental part.

Single crystals of **1** and **2** were grown by slow evaporation from a n-hexane/dichloromethane solution, respectively, which allow one to unveil their structural features through the X-ray single crystal analysis. Compound **1** adopts a nearly geometric plane surface (Fig. 3a), in which the heptagonal ring B induces the adjacent benzene ring out of the planarity with a dihedral angle of 21.9° (Fig. 3c), whereas the other seven-membered ring C features the planar structure. Accordingly, there are two different conformations in the solid state of **1**, that is, enantiomers *M* and *P* coexist with a ratio of 1:1 in the crystal (Fig. 3e). In comparison with **1**, compound **2** with an additional five-membered ring, displays a slightly saddle-shaped geometry, in which the heptagonal rings B and C induce the steric hindrance between their adjacent benzene rings E/F and G/H with the dihedral angles of 21.6° and 20.4°, respectively (Fig. 3b and 3d). In the packing pattern, compound **2** crystallizes along the *c*-axis of the unit cell with a pair of enantiomers (*M* and *P*) to establish columnar superstructures with a minimum interplanar space of 3.28 Å (Fig. 3f). Moreover, the X-ray analysis discloses the detailed bonding information of **1** and **2** (Fig. 3c and 3d), which also provide crucial information on the singlet biradical character for **2**.[30-32] The bond lengths in **1** reveal that the six-membered ring A (Fig. 3c) has two short C-C bonds (1.346 Å and 1.376 Å) and four long C-C bonds (1.437-1.463 Å), manifesting a pronounced bond alternation for the *p*-quinodimethane skeleton in **1**. For **2**, the intermediate value (1.407 Å, Fig. 3d) of bond *a* is substantially longer than that of **1** (1.370 Å) and the closed shell indeno[2,1-*c*]fluorene[40] (1.377 Å, Fig. S26), indicating the contribution of the open-shell resonance structure in the ground state of **2** (**2**-**1** in Fig. 1d); nevertheless, the bond length of *a* in **2** is shorter than that of the open shell indeno[2,1-*b*]fluorene[41] (1.437 Å, y_0 = 0.68, Fig. S26), coinciding the relatively smaller open-shell character of **2** (y_0 = 0.29).

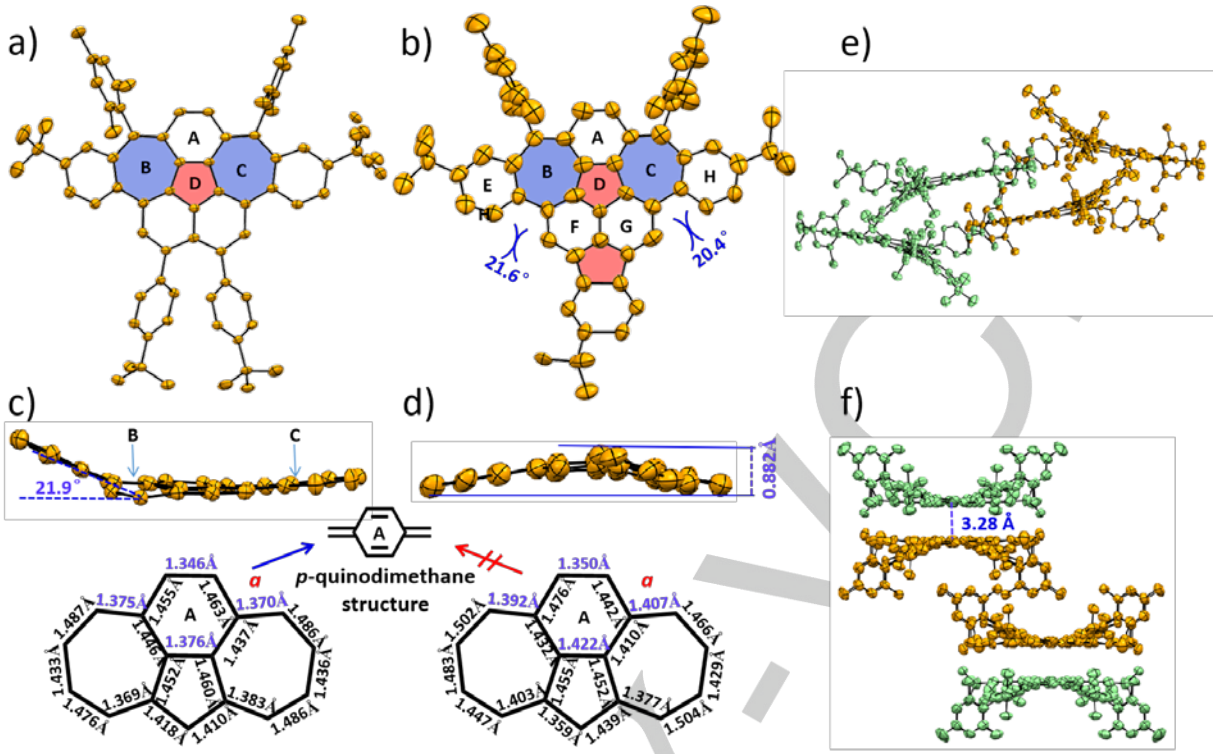

Figure 3. X-ray crystallographic molecular structures of **1** (a) and **2** (b). The hydrogen atoms are omitted for clarity. Side view of **1** (c) and **2** (d) as well as the bond lengths of the embedded 7-5-7 membered rings (the substituents in **1** and **2** are removed for clarity). (e, f) Crystal packing of **1** and **2**. Orange: *M*-enantiomer; Light green: *P*-enantiomer.

Moreover, the nucleus-independent chemical shift (NICS) calculations were performed at the GIAO-B3LYP/6-311+G(2d,p) level, to evaluate the aromaticity of each rings in these two nanographenes **1** and **2**. The obtained NICS $(1)_{zz}$ values of **1** were 13.5 and 9.4 for the heptagonal ring B and ring A (Fig. 4b), respectively, demonstrating their anti-aromatic feature, which is consistent with the X-ray structural analysis; while large negative values were found at the peripheral benzene rings E (−15.7) and F (−20.7). Accordingly, the paratropic character on the ring A and heptagons in **1** magnetically suppresses the aromatic character of the peripheral hexagons E and F. Thereby, compared to the aromatic dibenzo-corannulene with 6-5-6 membered ring (Fig. 4a), the 7-5-7 ring embedded nanographene **1** exhibits anti-aromatic nature. The values of rings A and B in **2** are comparable to **1** (Fig. 4c), however, the central five-membered ring D (−1.2) in **2** seems to behave as nonaromatic ring, in which the value is largely higher than that of in **1** (−14.1) (Fig. 4b). To further support the local aromaticity of 5-7-5 embedded nanographenes **1** and **2**, anisotropy of the induced current-density (ACID) analysis were evaluated (Fig. 4e and 4f). Continuous counterclockwise paratropic ring currents appeared around the 7-6-7 units (rings B-A-C) in the ACID plots of **1** and **2**. However, diamagnetic ring currents were found in other six-membered rings. These results indicate that the 7-6-7 rings (rings B-A-C) in **1** and **2** display anti-aromatic character, which is consistent with the results of NICS calculations.

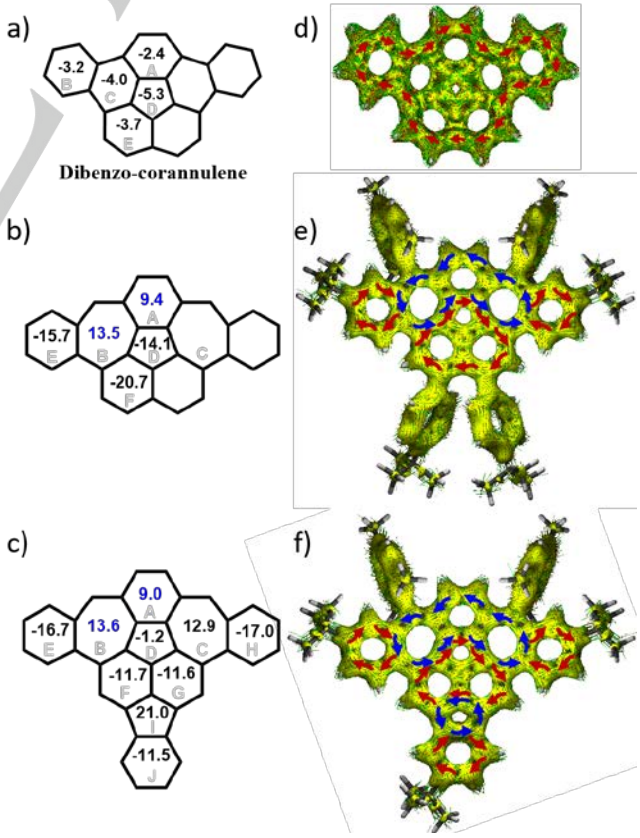

Figure 4. (a-c) $NICS(1)_{zz\text{-}avg}$ values of dibenzo-corannulene, **1**, and **2** (calculated at the GIAO-B3LYP/6-31+G(2d,p) level of theory. (d-f) Calculated ACID plots of

dibenzo-corannulene, **1**, and **2**. The isovalue is 0.05, and the diamagnetic (clockwise) and paramagnetic (counterclockwise) ring currents under the magnetic field parallel to the *z*-axis are highlighted by red and blue arrows, respectively.

Compounds **1** and **2** have excellent solubility in common organic solvents such as dichloromethane (DCM), tetrahydrofuran (THF), and toluene, etc. The UV-vis absorption spectra of **1** and **2** in DCM solutions are recorded in Fig. 5a. Compounds **1** and **2** display similarly shaped UV-vis absorption patterns. For instance, there are one major absorption peak at 310 nm and another absorption peak centralized at 520 nm with two shoulder peaks at 490 and 455 nm for **1**. Compound **2** exhibits a bathochromically shifted by 49 nm relative to that of **1**, with an absorption maximum peak at 569 nm and two shoulder peaks at 530 and 492 nm, respectively. Accordingly, the optical energy gap for **1** and **2** were determined to be 2.21 and 2.06 eV, respectively, from the onset of their UV-vis absorption spectra. Interestingly, the pink DCM solutions of compounds **1** and **2** were non-emissive when excited with UV light and even no detectable fluorescence was observed with excitation at their absorption maximum, which is also in agreement with their anti-aromatic character. Furthermore, the time-dependent UV-vis measurement was performed under ambient condition to investigate the stability of **1** and **2**. There are no significant changes of the absorption curves for **1** and **2** within one months (Fig. S18). The electrochemical behavior of **1** and **2** were investigated by cyclic voltammetry (CV) (Fig. 5b). Compound **1** shows two reversible oxidation waves with half-wave potentials $E_{1/2}^{ox}$ at 0.68 and 1.35 V (vs. Fc^+/Fc). However, compound **2** manifests two reversible oxidation waves with half-wave potentials $E_{1/2}^{ox}$ at 0.54 and 1.10 V, and one reversible reduction wave with half-wave potential ($E_{1/2}^{ox}$) at –1.36 V (*vs.* Fc^+/Fc). Thus, the HOMO energy levels are estimated to be –5.55 and –5.41 eV for **1** and **2**, respectively, based on the onset potentials of the first oxidation wave. The corresponding LUMO energy levels for **1** and **2** are calculated to be –3.34 and –3.35 eV**,** respectively, based on their optical energy gaps.

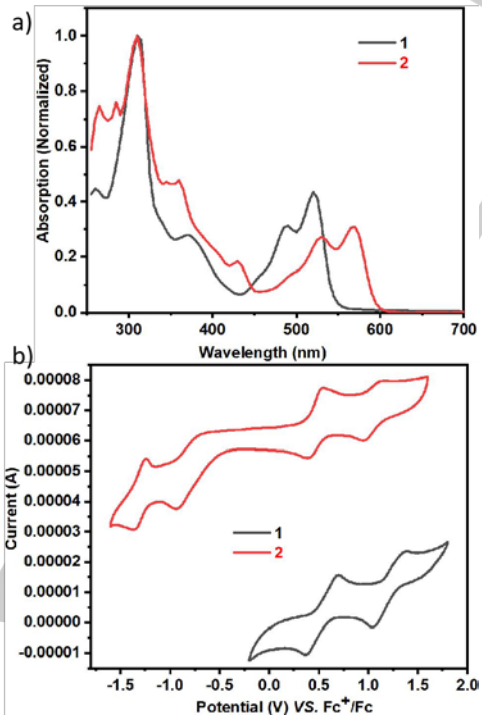

Figure 5. (a) UV-vis absorption spectra of **1** and **2** in DCM (1×10^{-5} mol/L). (b) Cyclic voltammetry of **1** and **2** in DCM containing 0.1 M nBu_4NPF_6 at a scan rate of 50 mVs^{-1}.

In summary, we have demonstrated the synthesis of two unprecedented nanographenes with seven-five-seven (7-5-7) membered rings. The crystallographic characterizations unambiguous display that while **1** adopts a nearly planar structure, compound **2** with an additional five-membered ring manifests a slightly saddle-shaped geometry. The structural analysis combined with the DFT calculations demonstrated that compounds **1** and **2** represent a new type of air-stable, fully conjugated anti-aromatic nanographenes with 7-5-7 membered rings, which can be used as potential candidates in optoelectronic devices. The synthetic strategy towards the defect engineering in nanographenes by building 7-5-7 membered rings can be applied to the construction of other air-stable and π-expanded nanographenes with anti-aromatic or open shell structures.

Acknowledgements

This work was supported by the Hong Kong Research Grants Council (HKU 27301720). J. Liu is grateful for the funding support from ITC to the SKL. Y. Fu thanks the Center for Information Services and High Performance Computing (ZIH) at TU Dresden for generous allocations of compute resources. We thank Prof. Dr. Y.-Z Tan (Xiamen University) for assistance in solving the X-ray crystal structure of **1** and Dr. K.-H. Low (The University of Hong Kong) for assistance in solving the X-ray crystal structure of **2**.

Keywords: polycyclic aromatic hydrocarbons • nanographenes • defects • seven-five-seven membered rings • aromaticity

[1] K. S. Novoselov, A. K. Geim, S. V. Morozov, D. Jiang, M. I. Katsnelson, I. V. Grigorieva, S. V. Dubonos, A. A. Firsov, *Nature* **2005**, 438, 197–200.

[2] X. Du, I. Skachko, F. Duerr, A. Luican, E. Y. Andrei, *Nature* **2009**, 462, 192–195.

[3] A. Narita, X. Y. Wang, X. Feng, K. Müllen, *Chem. Soc. Rev.* **2015**, 44, 6616–6643.

[4] A. K. Geim, K. S. Novoselov, *Nat. Mater.* **2007**, 6, 183–191.

[5] N. O. Weiss, H. Zhou, L. Liao, Y. Liu, S, Jiang, Y. Huang, X. Duan, *Adv. Mater.* **2012**, 24, 5782–5825.

[6] A. Narita, X. Feng, K. Müllen, *Chem. Rec.* **2015**, 15, 295–309.

[7] L. Talirz, P. Ruffieux, R. Fasel, *Adv. Mater.* **2016**, 28, 6222–6231

[8] A. Narita, Z. Chen, Q. Chen, K. Müllen, *Chem. Sci.* **2019**, 10, 964–975.

[9] A. Jolly, D. Miao, M. Daigle, J.-F. Morin, *Angew. Chem. Int. Ed.* **2020**, 59,4624–4633.

[10] F. Banhart, J. Kotakoski, A. V. Krasheninnikov, *ACS Nano* **2011**, 5, 26–41.

[11] O. V. Yazyev, S. G. Louie, *Nat. Mater.* **2010**, 9, 806–809.

[12] J. H. Warner, E. R. Margine, M. Mukai, A. W. Robertson, F. Giustino, A. I. Kirkland, *Science* **2012**, 337, 209–212.

[13] A. J. Stone, D. J. Wales, *Chem. Phys. Lett.* **1986**, 128, 501–503.

[14] A. Hashimoto, K. Suenaga, A. Gloter, K. Urita, S. Iijima, *Nature* **2004**, 430, 870–873.

[15] P. Y. Huang, C. S. Ruiz-Vargas, A. M. van der Zande, W. S. Whitney, M. P. Levendorf, J. W. Kevek, S. Garg, J. S. Alden, C. J. Hustedt, Y. Zhu, J. Park, P. L. McEuen, D. A. Muller, *Nature* **2011**, 469, 389–92.

[16] H. I. Rasool, C. Ophus, A.Zettl, *Adv. Mater.* **2015**, 27, 5771–5777.

[17] J. Liu, S. Mishra, C. A. Pignedoli, D. Passerone, J. I. Urgel, A. Fabrizio, T. G. Lohr, J. Ma, H. Komber, M. Baumgarten, C. Corminboeuf, R. Berger, P. Ruffieux, K. Müllen, R. Fasel, X. Feng, *J. Am. Chem. Soc.* **2019**, 141, 12011–12021.

[18] X. Yang, F. Rominger, M. Mastalerz, *Angew. Chem. Int. Ed.* **2019**, 58, 17577–17582 .

[19] X.-S. Zhang, Y.-Y. Huang, J. Zhang, W. Meng, Q. Peng, R. Kong, Z. Xiao, J. Liu, M. Huang, Y. Yi, L. Chen, Q. Fan, G. Lin, Z. Liu, G. Zhang, L. Jiang, D. Zhang, *Angew. Chem. Int. Ed.* **2020**, 59, 3529–3533.

[20] A. Konishi, K. Horii, D. Shiomi, K. Sato, T. Takui, M. Yasuda, *J. Am. Chem. Soc.* **2019**, 141, 10165–10170.

[21] Y. Han, Z. Xue, G. Li, Y. Gu, Y. Ni, S. Dong, C. Chi, *Angew. Chem. Int. Ed.* **2020**, 59, 9026–9031.

[22] N. Ogawa, Y. Yamaoka, H. Takikawa, K. Yamada, K. Takasu, *J. Am. Chem. Soc.* **2020**, 142, 13322–13327.

[23] K. Yamamoto, Y. Ie, N. Tohnai, F. Kakiuchi, Y. Aso, *Sci. Rep.* **2018**, 8, 17663.

[24] J. Ma, Y. Fu, E. Dmitrieva, F. Liu, H. Komber, F. Hennersdorf, A. A. Popov, J. J. Weigand, J. Liu, X. Feng, *Angew. Chem. Int. Ed.* **2020**, 59, 5637–5642.

[25] B. Pigulski, K. Shoyama, F. Würthner, *Angew. Chem. Int. Ed.* **2020**, DOI: 10.1002/anie.202005376.

[26] T. Kirschbaum, F. Rominger, M. Mastalerz, *Angew. Chem. Int. Ed.* **2020**, 59, 270–274.

[27] C. Zhu, K. Shoyama, F. Würthner, *Angew. Chem. Int. Ed.* **2020**, DOI: 10.1002/anie.202010077.

[28] S. Das, J. Wu, *Org. Lett.* **2015**, 17, 5854–5857.

[29] A. Shiotari, T. Nakae, K. Iwata, S. Mori, T. Okujima, H. Uno, H. Sakaguchi, Y. Sugimoto, *Nat. Commun.* **2017**, 8, 16089.

[30] C. K. Frederickson, B. D. Rose, M. M. Haley, *Acc. Chem. Res.* **2017**, 50, 977–987.

[31] G. E. Rudebusch, J. L. Zafra, K. Jorner, K. Fukuda, J. L. Marshall, I. Arrechea-Marcos, G. L. Espejo, R. P. Ortiz, C. J. Gomez-Garcia, L. N. Zakharov, M. Nakano, H. Ottosson, J. Casado, M. M. Haley, *Nat. Chem.* **2016**, 8, 753–759.

[32] J. Ma, K. Zhang, K. S. Schellhammer, Y. Fu, H. Komber, C. Xu, A. A Popov, F. Hennersdorf, J. J Weigand, S. Zhou, W. Pisula, F. Ortmann, R. Berger, J. Liu, X. Feng, *Chem. Sci.* **2019**, 10, 4025–4031.

[33] T. J. Seiders, E. L. Elliott, G. H. Grube, J. S. Siegel, *J. Am. Chem. Soc.* **1999**, 121, 7804–7813.

[34] T. Kubo, *Chem. Rec.* **2015**, 15, 218–232.

[35] T. Kubo, *Chem. Lett.* **2015**, 44, 111–122.

[36] Z. Zeng, X. Shi, C. Chi, J. T. L. Navarrete, J. Casado, J. Wu, *Chem. Soc. Rev.* **2015**, 44, 6578–6596.

[37] J. J. Dressler, M. M. Haley, *J. Phys. Org. Chem.* **2020**, e4114.

[38] J. J. Dressler, M. Teraoka, G. L. Espejo, R. Kishi, S. Takamuku, C. J. Gómez-García, L. N. Zakharov, M. Nakano, J. Casado, M. M. Haley, *Nat. Chem.* **2018**, 10, 1134–1140.

[39] J. J. Dressler, A. C. Valdivia, R. Kishi, G. E. Rudebusch, A. M. Ventura, B. E. Chastain, C. J. Gómez-García, L. N. Zakharov, M. Nakano, J. Casado, M. M.Haley, *Chem* **2020**, 6, 1353–1368.

[40] A. G. Fix, P. E. Deal, C. L. Vonnegut, B. D. Rose, L. N. Zakharov, M. M. Haley, *Org. Lett.* **2013**, 15, 1362–1365.

[41] A. Shimizu, R. Kishi, M. Nakano, D. Shiomi, K. Sato, T. Takui, I. Hisaki, M. Miyata, Y. Tobe, *Angew. Chem. Int. Ed.* **2013**, 52, 6076 –6079.

COMMUNICATION

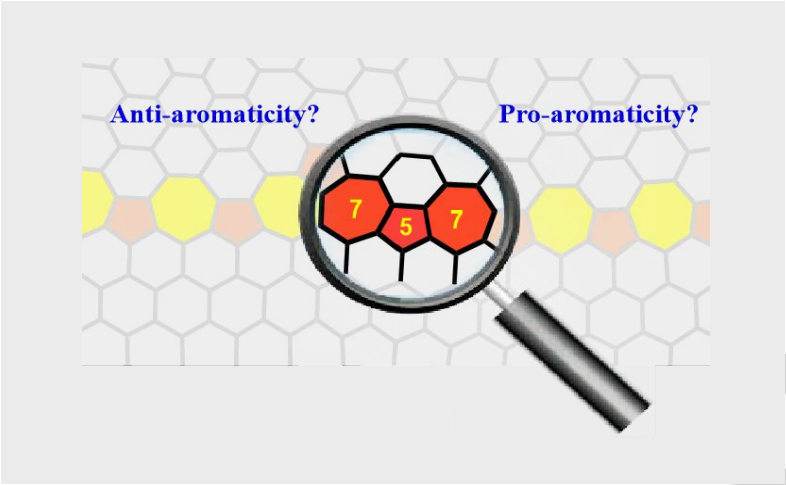

*Yiyang Fei, Yubin Fu, Zichao Li, Hartmut Komber, Shengqiang Zhou, Xinliang Feng, Junzhi Liu**

Page No. – Page No.

Defective Nanographenes with Seven-Five-Seven (7-5-7) Membered Rings: Anti-aromaticity or Pro-aromaticity?

Seven-Five-Seven (7-5-7) Membered Rings: Two novel nanographenes with seven-five-seven (7-5-7) membered rings were rationally designed and synthesized in this work, which provides a new line to synthesis of air-stable anti-aromatic nanographenes with non-alternant topology and enables control of their electronic structures.